Phase transformations and induced volume changes in a nitrided ternary Fe–3%Cr–0.345%C alloy

S. Jegou [a,b,*], L. Barrallier [a], R. Kubler [a]

[a] *MecaSurf Laboratory, Arts & Metiers ParisTech, Aix-en-Provence, France*
[b] *Aubert & Duval, Eramet Group*

Abstract

Phase transformations during nitriding of a ternary carbon iron-based alloy Fe–3%Cr–0.345%C were studied, aiming for a better understanding of residual stresses generation and evolution. The relationship between the precipitation of Cr_7C_3 carbides and CrN nitrides, the induced volume change and the mechanical properties were investigated at three distinct depths of the diffusion zone. The relaxation of residual stresses arose through phase transformations according to the diffusion of nitrogen but also of carbon.

Keywords: Nitriding; Iron alloys; Residual stresses; Phase transformations; Precipitation

1. Introduction

In integrated design, a residual stress state must be optimized in order to enhance the mechanical properties of a part, such as fatigue life, wear or corrosion resistance, and also to control residual macroscopic deformations to avoid additional machining. Nitriding is a well-established thermo-chemical treatment of iron alloys based on nitrogen diffusion [1]. The objectives lie in taking advantage of high hardening and internal stresses due to second phase strengthening [2]. This study deals with gas nitriding resulting in the formation of a two sub-layer surface: the compound layer composed of iron nitrides ε-$Fe_{2-3}N$ and/or γ′-Fe_4N, increasing the tribological properties and corrosion resistance [3], followed by the diffusion layer, where mainly sub-microscopic MN nitrides (M = Cr, V, Mo, ...) precipitate, ensuring fatigue and wear resistance [4].

Nitriding is an example where residual stresses arise through the generation of chemically induced misfits [5]. Understanding the generation of residual stress implies identifying misfits (or eigenstrains) between different regions or phases within one part. In the case of nitriding, knowledge of residual stress development is lacking owing to the complexity of the phenomenon. The precipitation of nitrides due to additional nitrogen atoms implies a volume increase in the surface (volumetric eigenstrain) balanced with the untransformed core material, resulting in compressive residual stress generation. Induced volume change finds its origins in coupled effects between lattice distortions, volume changes accompanying precipitation, thermal effects and chemical phase evolution [6–8]. A phenomenological approach of macroscopic residual stresses was recently made by Vives Diaz et al. [9] in the case of binary nitrided iron-based alloys according to the different regions of a nitrided surface exhibiting different kinds of precipitation of nitrides (semi- and incoherent, discontinuous). This approach is supported by the characterization of the nanometric precipitation by means of atom probe tomography [10]. The dependence of the residual stress gradient on nitriding conditions (time, temperature, nitriding potential) have been were fully characterized [11]. Stress relaxation was investigated during the treatment by in situ X-ray diffraction (XRD) analysis over the first

* Corresponding author. Address: MecaSurf Laboratory, Arts & Metiers Paris Tech, Aix-en-Provence, France.
E-mail addresses: sebastien.jegou@ensam.eu, jegou_sebastien@yahoo.fr (S. Jegou).

10 μm below the surface, concluding with stress relaxation by the superposition of thermally induced and precipitation-induced residual stresses, cooling having no influence on the diffusion zone [12,13]. No residual plastic straining takes place through the diffusion surface after nitriding [14]. The influence of post-treatment loading on diffusion was also investigated and concluded with a thinner diffusion layer with higher compressive residual stresses [15].

In order to predict residual stress, some attempts were made to model nitriding based on diffusion of nitrogen considering the precipitation of MN nitrides and linked to a mechanical model. But all these models, which are often available for binary iron-based alloys, only determine a global stress state and need some assumptions based on either the diffusion of carbon (fraction of cementite) or phenomenological stress-relaxation equations based on a thermal creep phenomenon [16–19].

In the case of carbon iron-based alloys, incoherent nitrides are formed by the transformation of initial carbides [20,21]. Diffusion of the released carbon is usually reported during nitriding, with decarburization of the close surface and carbon enrichment at the nitrogen diffusion front [15,22]. Carbon generally drives cementite precipitation at grain boundaries parallel to the nitrided surface through the diffusion layer [22,23]. However, any metallurgical relations between these observations and residual stress evolution have not been totally exploited, limiting understanding to a complex interaction between nitrogen and carbon atoms and the correlation of experimental observations between the decarburization of the surface with the decreasing residual stress at the beginning of the diffusion layer [7,18]. Moreover, even if the coherent precipitation zone exhibits similar microstructure evolution across the depth in terms of nitride size and volume fraction [20,24,25], the gradient of residual stresses can still not be explained, since no discontinuous precipitation zone is observed as in the case of iron-based alloys.

Thus, a nitrided layer is not homogeneous, and the microstructure has to be characterized in term of volume change evolution according to nitrogen and also carbon diffusion. Carbon is a key point not considered enough and too often neglected in residual stress generation and evolution. Competition with residual stress relaxation through a controlled creep phenomenon is not yet fixed. Indeed, carbide transformation during nitriding has not been considered in the estimation of volume change.

This work deals with phase transformations and induced volume changes according to nitrogen and carbon diffusion during the nitriding process. It aims for a better understanding of residual stress development and prediction of volume heterogeneities for a multi-scale numerical model, taking into account micro–macro scale effects [6,26–28]. This paper deals with the study of a ternary low-carbon iron-based alloy Fe–3%Cr–0.345%C. The microstructures of three typical depths of the diffusion zone were investigated.

2. Experimental procedure

2.1. Material and nitriding process

Specimen elaboration and nitriding treatments were carried out by Aubert & Duval. Specimens were from an iron-based alloy with 0.35 wt.% C and 3 wt.% Cr, quenched and annealed at 590 °C. They were then nitrided for different times (10, 50 and 100 h) and temperatures (500, 520 and 550 °C) for a given nitrogen potential. All specimens were ground and polished for the purpose of optical microscopy and chemical analyses. Composition profiles were carried out by electron probe microanalysis analysis (EPMA) using a Cameca Electron Microprobe SX100 with accelerating voltage 10 kV and current 100 nA. Profiles were obtained across the sections with single measurement points every 15 μm. For better quantification of carbon, glow discharge optical emission spectrometry (GDOES) was also performed along the depth of the specimens.

2.2. Phase characterization using XRD

X-ray phase analyses were carried out using a Siemens D500 diffractometer with Cr K_α radiation ($\lambda = 0.228975$ nm). Scanning conditions were in the range $40° \leqslant 2\theta \leqslant 140°$ with a step size of 0.032° in 2θ and step time 300 s. The JCPDS database was used for phase identification [29].

2.3. Microstructural characterization

Optical microscopy investigations were performed prior to any analysis to ensure the quality of nitriding. Specimens were etched with 3% nital (3 ml HNO_3, 97 ml ethanol). They were observed using a Leitz Aristomet optical microscope and a JEOL JMS 6400 scanning electron microscope.

Transmission electron microscopy (TEM) samples were machined using focused ion beam (FIB) sample preparation [30]. Films were directly prepared on sample cross sections at the desired depths and thinned down to 50 nm. TEM observations were carried out using a JEOL JEM 2010F, and sample preparations with a Philips FIB 200 TEM instrument.

Image analysis was performed using ImageJ software. The sizes of the precipitates were determined using the equivalent calculated diameters, and the standard deviations obtained were used to determine the confidence interval.

2.4. Hardness measurements

Hardness-depth profiles were obtained using a Leica VMHT device. Loading was chosen as 1.98 N with a 15 s loading time. Three indents were performed at each depth of a cross section, respecting a distance of three times the indent size in order to avoid interactions between indents. The given hardness $\Delta HV(z) = HV(z) - HV(\text{core})$ corre-

sponds to the difference between the depth z and the non-affected core material.

2.5. Stress analysis using XRD

Residual stresses were determined using a Siemens D500 diffractometer with Cr K_α radiation ($\lambda = 0.228975$ nm) on the {2 1 1} diffracting plane of α-iron. The gauge volume was determined with a 3-mm diameter tape mask. The $\sin^2 \Psi$ method was used to determine the mean residual stresses ($\sigma_{XX} - \sigma_{ZZ}$) in the ferritic matrix (multiphase material) along the nitrided depth (z axis). Depth profiles were obtained using electro-chemical surface layer removal. The mean residual stresses were normalized according to the maximal compressive stress found.

3. Results

3.1. Nitrogen and carbon concentration depth profiles

Fig. 1 shows the nitrogen content-depth profiles (EPMA) according to time and temperature of nitriding. Increasing time involves deeper nitrogen diffusion. The nitrogen content stays nearly constant through the diffusion layer. The temperature activates the diffusion of nitrogen, and a slight decrease in the content can be observed at 550 °C, but stays within a range of 0.1%. Carbon content-depth profiles (GDOES) for 10 and 100 h at 550 °C are given in Fig. 2. Decarburization of the surface (30 and 85 μm, respectively) was observed as well as an enrichment of carbon at the end of the diffusion layer.

3.2. Microstructure of nitrided surfaces

Nitrided specimens present the same morphology observed on the light optical micrographs (Fig. 3). The compound layer is 25–30 μm thick. The diffusion layers have a similar morphology exhibiting a martensitic structure.

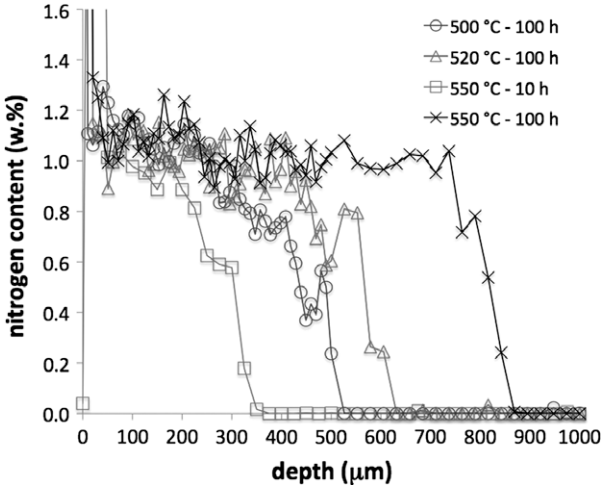

Fig. 1. Influence of process temperatures and times on nitrogen diffusion of nitrided Fe–3%Cr–0.35%C (EMPA analyses).

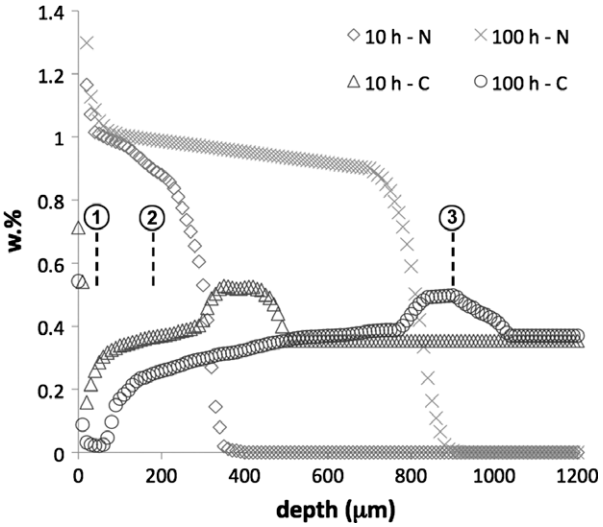

Fig. 2. Nitrogen and carbon in-depth profiles of Fe–3%Cr–0.35%C nitrided at 550 °C (GDOES analyses). Three investigated depths of the diffusion zone are highlighted: (1) 55 μm; (2) 175 μm; and (3) 920 μm.

Porosity at grain boundaries up to a depth of 100 μm was observed after 100 h nitriding at 550 °C (Fig. 3d). Moreover, backscattered SEM observations also indicate a higher precipitation of cementite at grain boundaries close to the surface after 10 h at 550 °C, whereas this was less significant deeper in the diffusion zone after 100 h nitriding.

3.3. Hardness profiles

Hardness profiles show similarities to diffusion profiles according to process times and temperatures (Fig. 4). Increasing time involves slight changes in regions experiencing nitriding, whereas hardness increased deeper in the nitrided surface. Temperature has a more pronounced effect, increasing the diffusion coefficient of nitrogen and so the nitrided depth. A decrease of 150 HV at a depth of 50 μm was measured between 10 and 100 h at 550 °C, but only 20 HV at 520 °C, suggesting temperature controlled annealing phenomena.

3.4. Residual stress–depth profiles

Mean residual stresses over the ferritic matrix $\sigma_{XX} - \sigma_{ZZ}$ are presented in Fig. 5. Depending on times and temperatures, the gradient of residual stresses was modified during the treatment. The compound layer and the interface with the diffusion layer can exhibit tensile stresses. During nitriding, residual stresses between the surface and the depth of the maximal stress are decreasing. Increasing temperature involves a decrease in residual stresses which was significant at the beginning of the treatment. In the case of 100 h nitriding at 550 °C, the first hundred micrometres even exhibits compressive stresses after being under tensile or low stresses for 10 and 50 h. The minimal residual stress depth (30 and 85 μm for 10 and 100 h, respectively) corresponds to the decarburization depth in Fig. 2.

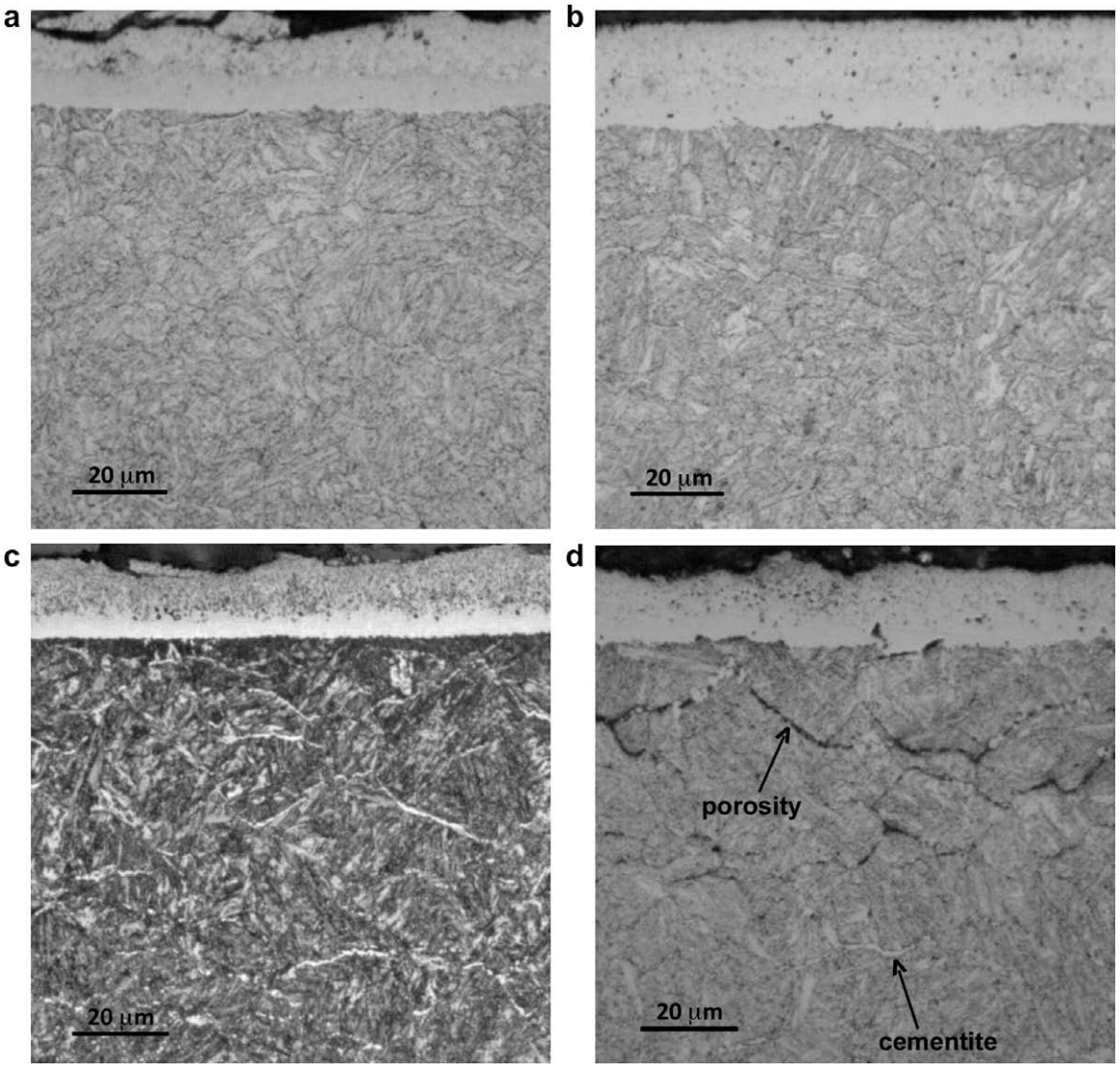

Fig. 3. Optical micrographs of the nitrided surface of Fe–3%Cr–0.35%C depending on process times and temperatures: (a) 100 h/500 °C; (b) 100 h/520 °C; (c) 10 h/550 °C; and (d) 100 h/550 °C.

3.5. Metallurgy within the diffusion zone

Owing to notable differences according to previous characterizations and temperature effects, three depths of the diffusion zone of specimens nitrided for 10 and 100 h at 550 °C (see Fig. 2) were investigated (XRD, SEM and TEM). These depths are characteristic of the kinetics of residual stress development during nitriding. They correspond to the interface between the compound and diffusion layers (55 μm), the depth of the maximal compressive stress after 10 h (175 μm) and the carbon enrichment depth after 100 h (920 μm). The nature of the phases present was analysed in order to understand the origin of stress generation and volume change of each phase.

3.5.1. Interface between compound and diffusion layers (CD interface)

XRD and SEM imaging using backscattered electrons revealed the presence of two distinguishing phases at the grain boundaries, identified as either cementite Fe_3C for 10 h nitriding or iron nitride Fe_4N in the case of 100 h treatment (Fig. 6). TEM investigations (Fig. 7) correlate these observations and indicate that cementite at the grain boundaries was polycrystalline, the grains having a 300–400 nm diameter. A very fine precipitation of CrN nitrides with a diameter <20 nm was distributed in the matrix as in the vicinity of grain boundaries (Fig. 7a). This fine precipitation was also present after 100 h at the grain boundaries, and cementite was replaced by the iron nitride Fe_4N (Fig. 7b).

3.5.2. Maximum of compressive stress after 10 h

The microstructure after 10 and 100 h nitriding was investigated at a depth of 175 μm, which corresponds to the maximal compressive stress depth after 10 h. XRD analyses indicated the presence of ferrite, chromium nitride CrN and cementite. Nevertheless, owing to the minimum 3% volume fraction that can be assessed by classical XRD, TEM observations were carried out, particularly in

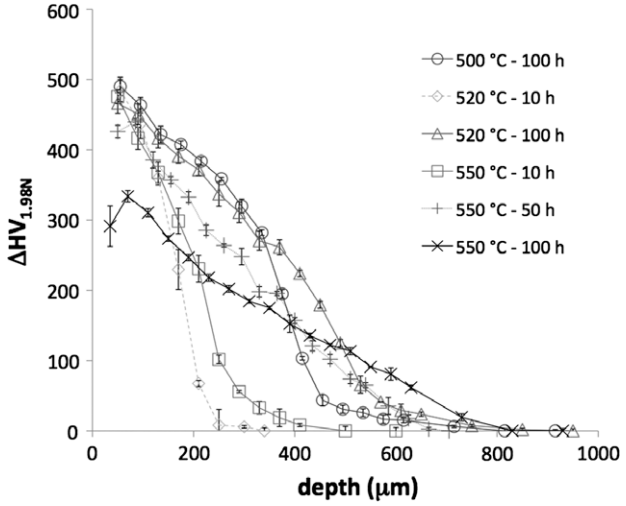

Fig. 4. Influence of process time and temperature on hardness–depth profiles of nitrided Fe–3%Cr–0.35%C. Hardness values are given as $\Delta HV(z) = HV(z) - HV(\text{core})$.

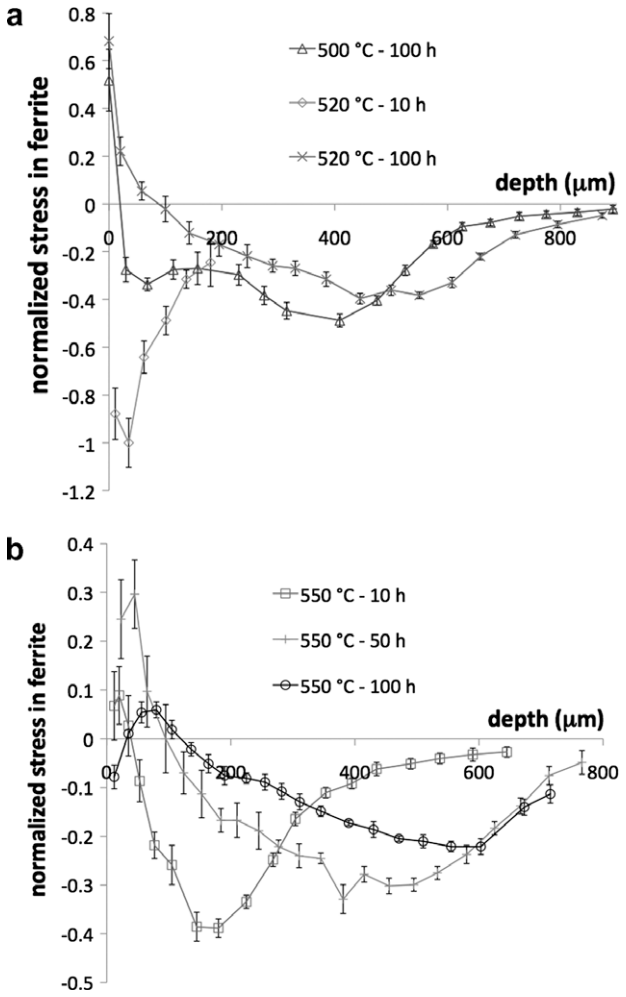

Fig. 5. Influence of process time and temperature on residual stress–depth profiles of nitrided Fe–3%Cr–0.35%C. Mean stresses over the ferritic matrix $\sigma_{XX} - \sigma_{ZZ}$ analysed by XRD using the $\sin^2 \Psi$ method. Mean stresses are normalized according to the maximal compressive stress: (a) 500 and 520 °C and (b) 550 °C.

the case of short 10 h nitriding. Fig. 8 shows the presence of inter-granular Cr_7C_3 carbides with a diameter of 100–150 nm in addition to fine CrN nitrides and cementite. However, no Cr_7C_3 carbides at such depths were found after 100 h nitriding, suggesting complete transformation.

3.5.3. End of the diffusion layer

The end of the diffusion layer was characterized by an increase in carbon content (Fig. 2). The influence on carbide precipitation was investigated by TEM, in particular for long nitriding times. Fig. 9 shows an example of the microstructure at a depth of 920 μm in the case of 100 h nitriding. Precipitates were identified as Cr_7C_3 carbide and exhibited a diameter of 86 nm (±7 nm), with a non-negligible number of them having a size of 120–240 nm (Fig. 10). The unaffected material was also investigated for comparison, and the mean equivalent diameter was equal to 45 nm (±3 nm) (Fig. 10). Therefore the quantity of Cr_7C_3 carbides was increasing in front of the diffusion front during nitriding due to the carbon enrichment. This suggests a depletion of chromium in the ferritic solid solution.

4. Discussion

4.1. Calculation of volume change

During nitriding, heterogeneities exist at the microscopic scale due to the diffusion of nitrogen and the resulting chemical and microstructural gradient (Fig. 11). Therefore the heterogeneities of local eigenstrains divided into plastic, thermal and structural dilatation due to phase transformations ($\dot{\varepsilon}_l = \dot{\varepsilon}_p + \dot{\varepsilon}_{th} + \dot{\varepsilon}_{vol} + \ldots$) induce residual stresses that take place in macroscopic residual stress generation. These heterogeneities must be described in order to build mechanical models aimed at integrated design. This approach is of importance when the complex geometry of mechanical parts has to be taken into account because of modifying the diffusion of nitrogen and developing a triaxial stress state [26,31].

A volume change calculation was proposed in agreement with a mechanical model of nitriding under development [6,28], but also in agreement with XRD analysis, which determined the mean residual stress $\sigma_{XX} - \sigma_{ZZ}$ in the ferritic phase ($\sin^2 \Psi$ method). The mechanical model, based on a self-consistent scheme with n phases (ferrite and $n-1$ precipitates), is governed by volumetric eigenstrain, and so the determination of the volume changes due to the precipitation. The volume change calculation is based on a comparison of the volume of precipitates at a given time and depth with the volume of precipitates at a second time. The specific volume $\upsilon_{\Phi i}(T)$ and the volume of precipitates $V_P(T)$ were determined at a given temperature T as follow:

$$\upsilon_{\Phi i}(T) = \frac{V_{lattice}(T) \cdot A}{\sum_{j=1}^{q} N_{\Phi i}^{Zj} \cdot M^{Zj}} \quad \text{and}$$

$$V_p(T) = m(T) \cdot \sum_{i=2}^{n} \upsilon_{\Phi i}(T) \cdot \omega_{\Phi i}(T)$$

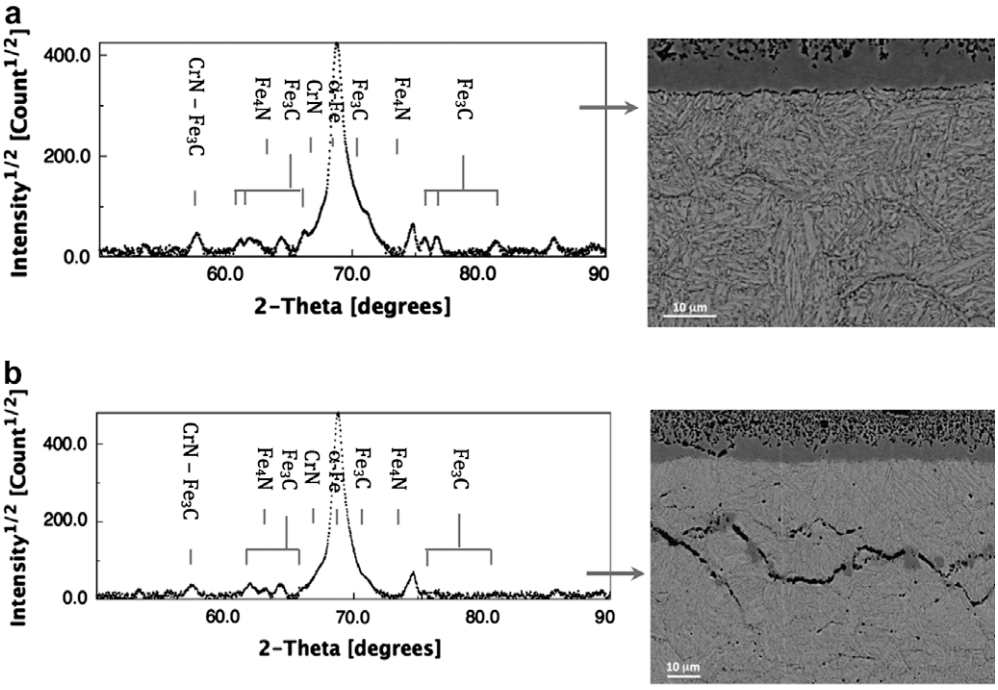

Fig. 6. Compound–diffusion interface (55 µm depth): XRD analyses and SEM imaging using backscattered electrons of Fe–3%Cr–0.35%C nitrided at 550 °C for: (a) 10 and (b) 100 h. After 10 h, Fe_4N was observed to a depth of 30 µm, whereas it was present to a depth of 70 µm after 100 h. Picks not indicated come from a tape mask for limiting gauge volume.

where $V_{lattice}(T)$ is the elementary volume of phase Φ_i, which takes into account lattice variations with the chemical composition of the phase and also temperature T, A is Avogadro's number, $N_{\Phi i}^{Zj}$ is the stoichiometric coefficient of element Z_j in phase Φ_i, M^{Zj} is the molar weight of element Z_j, $m(T)$ is the total mass of the system, and $\omega_{\Phi i}(T)$ is the weight fraction of phase Φ_i before nitriding at temperature T. Thermo-chemical data were obtained using Thermo-Calc software [32].

While new elements were added to the system due to nitrogen and carbon diffusion, the mass increase $\Delta m(T)$ between time $t-1$ and t is calculated assuming that heavy elements p (Fe, Cr, V, ...) do not diffuse during the treatment. Defining the quantity of heavy elements $\omega^{Zj}(T)$ at $t-1$ and $\omega'^{Zj}(T)$ at t, the mass increase and the new volume of precipitates $V'_P(T)$ at the temperature T are

$$\Delta m(T) = m(T) \cdot \left[\left(\sum_{j=1}^{p} \omega^{Zj}(T) \Big/ \sum_{j=1}^{p} \omega'^{Zj}(T) \right) - 1 \right] \quad \text{and}$$

$$V'_p(T) = (m(T) + \Delta m(T)) \cdot \sum_{i=2}^{n} \upsilon_{\Phi i}(T) \cdot \omega'_{\Phi i}(T)$$

Supposing a complete reaction of alloying elements with nitrogen and carbon atoms, and because of the presence of iron atoms in precipitates, the volume fraction can be calculated as follows, depending on the mass of iron in precipitates $m_{Fe}(T)$ at time $t-1$ and $m'_{Fe}(T)$ at time t:if iron atoms contribute to the precipitation $(m'_{Fe}(T) > m_{Fe}(T))$

$$\left.\frac{\Delta V}{V}\right|_P (T) = \frac{V'_P(T)}{V_P(T) + V_{Fe \to P}(T)} - 1$$

if a dissolution of precipitates occurs $(m'_{Fe}(T) < m_{Fe}(T))$

$$\left.\frac{\Delta V}{V}\right|_P (T) = \frac{V'_P(T) + V_{P \to Fe}(T)}{V_P(T)} - 1$$

where $V_{A \to B}$ is an equivalent volume of phase A transformed into phase B.

Finally, according to a mechanical assumption that the volume change of the matrix is negligible compared with precipitation, the volume change accompanying the precipitation at the temperature T can be written as follow in any previous case:

$$\left.\frac{\Delta V}{V}\right|_P (T) = y_P(T) . \frac{y'_P(T) . y_{Fe}(T) - y_P(T) . y'_{Fe}(T)}{y_P(T) . y'_{Fe}(T)}$$

where $y_{\Phi i}(T) = V_{\Phi i}(T)/V(T)$ is the volume fraction of phase Φ_i at the temperature T.

For the purpose of the micro-mechanical model, the volumetric eigenstrain at the temperature T is then calculated:

$$\dot{\varepsilon}_{vol} = \dot{y}_P(T) \cdot \frac{1}{3} \cdot \left.\frac{\Delta V}{V}\right|_P (T) \cdot \mathrm{I}$$

where $\dot{y}_P(T)$ is the volume fraction rate of precipitates according to the transformations, and I is the second-order identity tensor.

4.2. Interpretation of volume change

Characterizing the metallurgy of some typical depth of a nitrided surface shows direct links between chemical modifications and the distribution of residual stresses during nitriding. In this work, the interest is focused mainly on

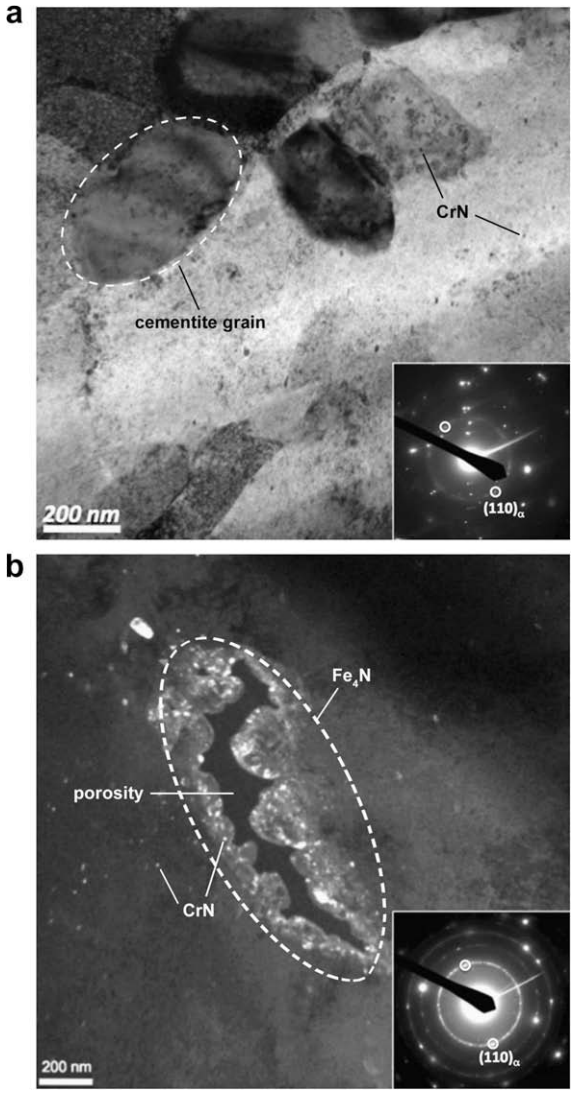

Fig. 7. Compound–diffusion interface (55 μm depth): TEM micrographs of Fe–3%Cr–0.35%C nitrided at 550 °C for (a) 10 h (bright field mode) and (b) 100 h (dark field mode) exhibiting polycrystalline cementite and Fe_4N precipitation at grain boundaries, respectively.

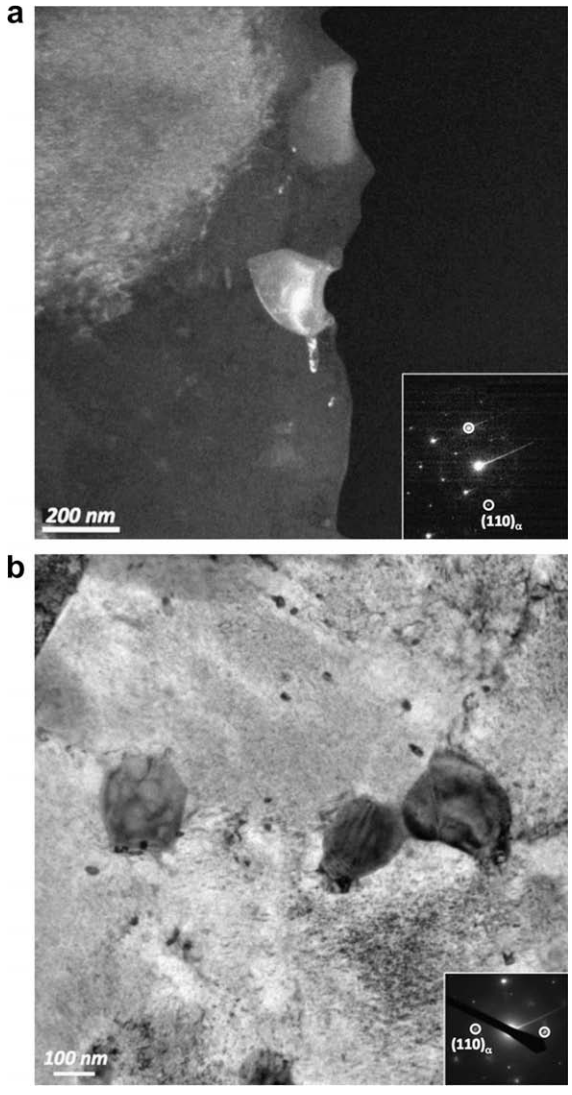

Fig. 8. TEM micrographs of Cr_7C_3 carbides at the maximal compressive stress depth (175 μm) in the case of Fe–3%Cr–0.35%C nitrided at 550 °C for 10 h: (a) dark field mode and (b) bright field mode.

the diffusion zone and also the interface between the compound and diffusion layers. The compound layer was only considered when formed as fixing the nitrogen flux of the diffusion zone. The process of nitriding and the resulting evolution of residual stress gradient can be described as follows:

(a) Precipitation of CrN nitrides: at the beginning of the treatment, as nitrogen is diffusing through the surface, fine semi-coherent CrN nitrides precipitate from the ferritic solid solution of chromium owing to its high nitrogen affinity. A significant increase in hardness is commonly observed (Fig. 4). Moreover, high compressive residual stress develops, as in the case of nitriding at 520 °C for 10 h, since this transformation gives the maximal volume change (Fig. 5). Indeed, this precipitation corresponds to the maximal difference of specific volume[1] between two phases through a nitrided surface (Table 1).

(b) Initial carbides transformed into nitrides: when nitrogen diffusion is carried out, the transformation of carbides into incoherent nitrides occurs, causing less volume change due to a smaller specific volume difference and also a decrease in the nitriding kinetic. In parallel, the released carbon drives cementite precipitation at the grain boundary. Moreover, Ginter et al. found that the atomic fraction of iron in substitutions in CrN nitrides was smaller than that in initial carbides [33]. Therefore, the transformation of carbides into nitrides is assumed to be more complex, with a

[1] The term "molar volume" should be more appropriate. But for better understanding of the volume change accompanying precipitation and because of changing in the same way, the "specific volume" of phases was used.

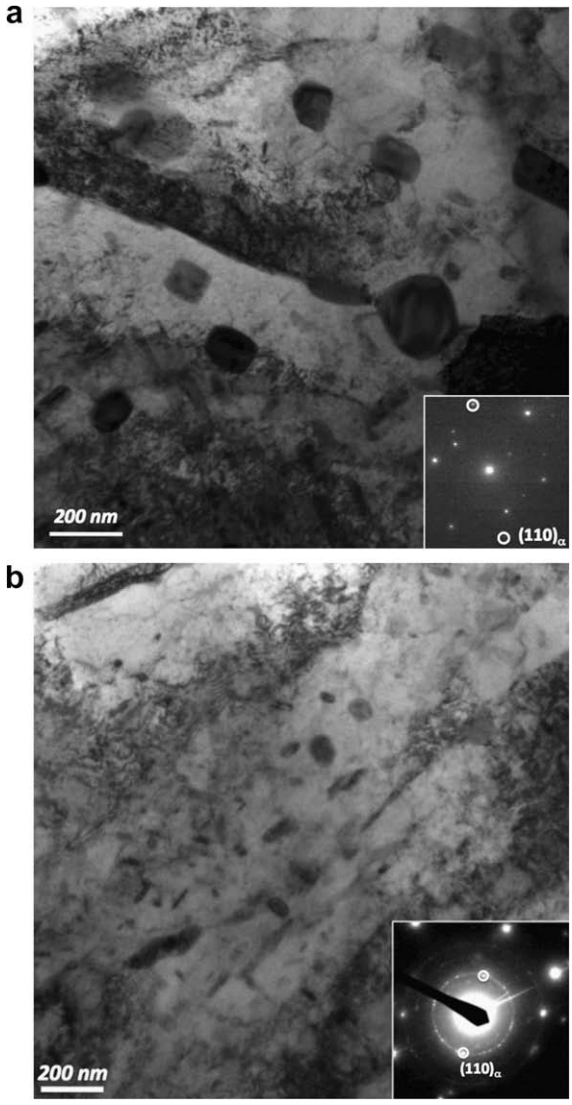

Fig. 9. Bright field TEM micrographs (a) at a depth of 920 μm and (b) of the core of Fe–3%Cr–0.35%C nitrided at 550 °C for 100 h. Carbides are identified as Cr_7C_3 type.

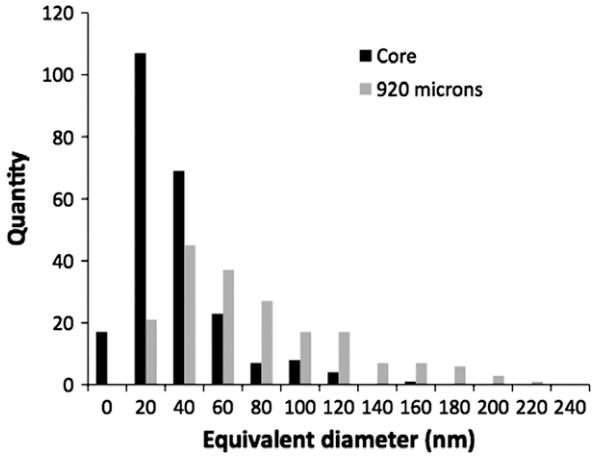

Fig. 10. Size distribution of precipitates corresponding to a depth of 920 μm and the core material in the case of Fe–3%Cr–0.35%C nitrided at 550 °C for 100 h. The total number of analysed precipitates was 188 and 236, respectively.

coupled transformation into cementite or dissolved iron atoms, in particular at grain boundaries [21]. This results in a much lower relative volume change if only a transformation into nitrides is considered. Finally, if carbon atoms diffuse toward the diffusion front, the volume fraction of precipitates decreases locally, resulting in a negative volumetric eigenstrain and thus a decrease in residual stresses. This is exactly what was observed experimentally at the maximal stress depth after 10 h of nitriding (Fig. 5b).

(c) Diffusion of carbon at the diffusion front: carbon is also free to diffuse at grain boundaries toward the end of the diffusion layer. This is characterized by an increase in the carbide size (Fig. 10), driving a depletion of alloying elements in the ferritic solid solution. Therefore, during the process, the quantity of semi-coherent nitrides decreases, and the quantity of incoherent nitrides from the transformation of carbides increases. According to assumptions (a) and (b), a decrease in residual stress (less volume change) is predicted deeper in the nitrided layer when process time increases. Experimental work shows such behaviour.

(d) The compound–diffusion layers interface: the decarburization of the interface involves a lower precipitation of cementite and even dissolution according to the carbon depth profile in Fig. 2. It results in a decrease in compressive residual stresses. Oettel et al. [7] also suggested the important influence of cementite in stress generation. Moreover, if the intragranular quantity of alloying element tends to be negligible, nitrogen atoms diffuse mainly along the grain boundaries, which leads to an increase in the local content of nitrogen. According to the Thermo-Calc calculation, cementite can be so replaced by iron nitrides from 1.5 wt.% N. Such a transformation involves positive volume change due to the specific volume difference and so explains the new increase in residual stresses after 100 h of nitriding in such regions that have already experienced stress relaxation up to 50 h. The transformation of cementite into an iron nitride was also proposed by Mittemeijer et al. [34].

(e) Influence of residual stresses on diffusion: cementite precipitation is clearly affected by the level of stress during nitriding. As the process time increases, the level of residual stresses decreases and cementite at grain boundaries is less significantly deep in the diffusion zone. Since cementite is oriented according to the developed plane stress state [19], it supposes a lower segregation of carbon at grain boundaries parallel to the nitrided surface. Residual stresses act to activate forces for short or long diffusion.

In order to illustrate these explanations, the experimental nitrogen and carbon content-depth profiles were used as

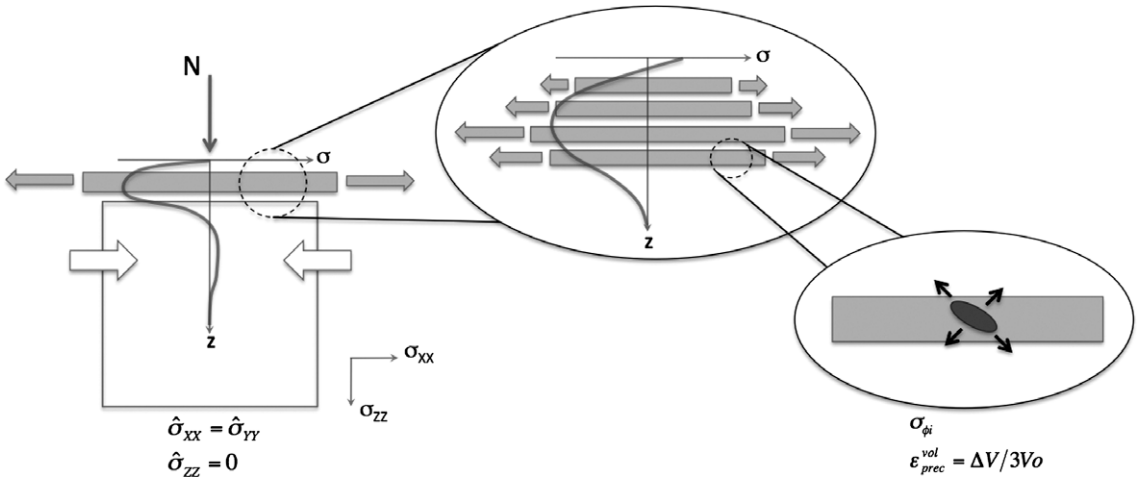

Fig. 11. Scheme of residual stresses generation during nitriding at different scales. Phase transformation effect at the nitriding temperature.

Table 1
Main phases found in a nitrided surface of carbon iron-based alloys; phase parameters according to the JCPDS database [29].

Phase	Structure	*a* (nm)	*b* (nm)	*c* (nm)	*v* ($cm^3\ kg^{-1}$)
α-Fe	Cubic	0.28664	–	–	127.06
CrN	Cubic	0.4140	–	–	161.29
Fe_3C	Orthorhombic	0.50910	0.67434	0.45260	130.38
$Cr_{23}C_6$	Cubic	1.06599	–	–	144.93
Cr_7C_3	Orthorhombic	0.7019	1.2158	0.426	
Fe_4N	Cubic	0.3791	–	–	138.89
Fe_3N	Hexagonal	0.2695	–	0.4362	

input data in the proposed volume change calculation. The composition and weight fraction of each phase along the depth were determined using the Thermo-Calc software (Fig. 12). An increase in the fraction of carbides was predicted according to the enrichment of carbon at the diffusion front, as observed experimentally. Fig. 13 presents the total volume change accompanying the precipitation after 10 h nitriding at 550 °C. Owing to nitrogen and carbon diffusion, a gradient of volumetric eigenstrains is well predicted, with a maximum that corresponds to the maximal volume fraction of precipitates and residual stresses. If the 10 h thermo-chemical state is taken as reference, the corresponding evolution after 100 h nitriding at 550 °C is given for comparison. A negative volume change was found in the first two hundredth microns in parallel with the decrease in the volume fraction of precipitates after 100 h, assuming the generation of tensile residual stresses. The negative volume change presents a minimal value which suggests a minimal residual stress around a depth of 50 μm that is experimentally observed. At a depth of 300 μm, there is a corresponding volume change equal to zero, and so an equivalent residual stress state after 100 h is assumed and is experimentally observed. Between 300 and 500 μm, the volume loading decreases due to the increased carbides fraction, assuming less volume change when transformations occur after 10 h. Deeper than 500 μm, the 100 h volume change is comparable with 10 h; as nitrogen and

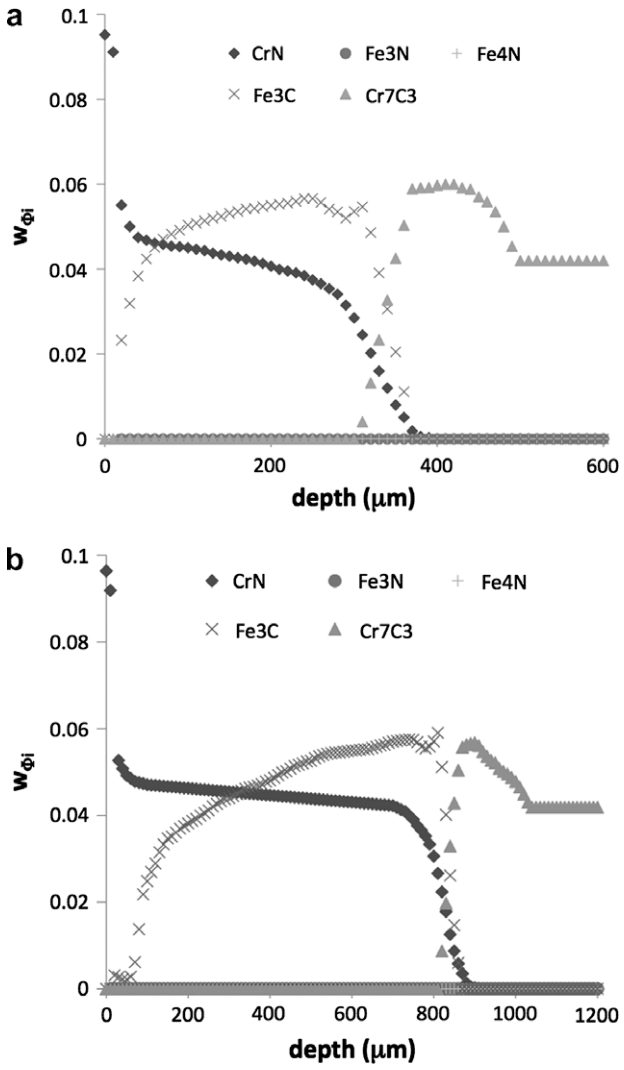

Fig. 12. Results from Thermo-Calc calculations based on experimental nitrogen and carbon content profiles. Case of Fe–3%Cr–0.35%C nitrided at 550 °C for (a) 10 h and (b) 100 h.

carbon evolution in such region were not considered, the volume change was calculated according to the initial state

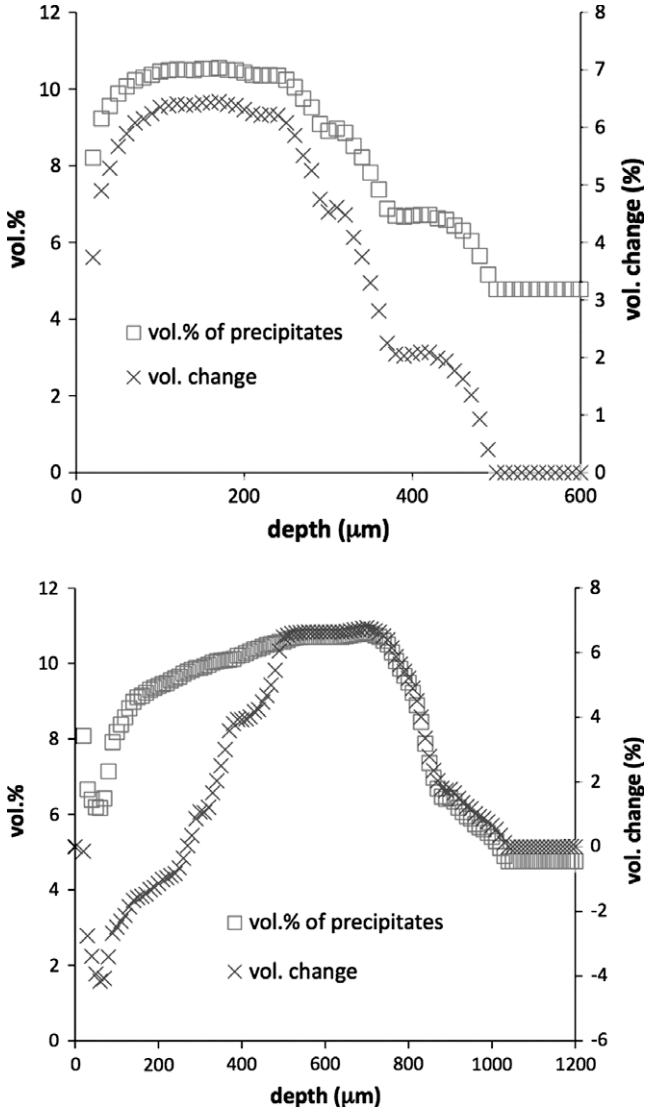

Fig. 13. Total volume fraction of precipitates and respective volume change according to experimental nitrogen and carbon-depth profiles and the proposed volume change calculation. Case of Fe–3%Cr–0.35%C nitrided at 550 °C for (a) 10 h and (b) the corresponding relative evolution after 100 h.

of the core material and so is maximal. Although these results were limited by the Thermo-Calc calculations done at complete thermodynamical equilibrium and a non-complete evolution of carbon diffusion, in particular at the interface between the compound and diffusion layer until 10 h, previous experimental assumptions were highly correlated by these results.

Concerning annealing phenomena, in particular at 550 °C, one can see in Fig. 4 that up to 50 h nitriding, the hardness depth profile stays quite unchanged, whereas a non-negligible decrease in residual stresses is observed. Moreover, a decrease in hardness between 50 and 100 h was measured to a depth of 400 μm. However, compressive residual stresses increase where the decrease in hardness is maximal near the close surface and, in contrast, decrease when hardening stays quite unchanged around a depth 400 μm. Therefore, annealing phenomena were not sufficient to describe the evolution of residual stresses during nitriding. The decrease in hardness could be attributed to the decrease in nitrogen flux in the close surface due to the precipitation of Fe_4N at the grain boundaries and so favours the growing of precipitates. Such an assumption about the nitrogen flux was also made to explain the growth of nitrides deeper in the diffusion zone where the nitrogen flux was low [24,25].

Finally, these results actually suggest that a nitrided surface was under volumetric loading–unloading cycles during the treatment. Residual stress relaxation, which is usually described using a thermally controlled creep phenomenon due to the couple diffusion–stress during nitriding [18,19], appears to be the effect of the complex transformation of carbides into nitrides. Volume changes being the activation forces of stress generation, the level of stress was determined mainly by the hardening law linked to fine semi-coherent nitrides [24,33], whereas the distribution of residual stresses through the surface depends on thermo-chemical evolution, which is a function of nitrogen, but also carbon diffusion. Process parameters thus play a role in the diffusion of light elements, kinetics of precipitation and, finally, thermodynamic parameters such as the atomic composition of each phase, balancing the mechanical properties of a nitrided surface through the volume change accompanying precipitation.

5. Conclusions

A nitrided ternary Fe–3%Cr–0.345%C alloy was investigated with respect to different process times and temperatures. Experimental observations and modelling were linked in order to acquire knowledge about residual stress generation and evolution during nitriding. Correlations between thermo-chemical modifications during the treatment of nitriding and the development of residual stresses were done through volume change modifications:

1. Residual stress gradient arises through heterogeneities of volumetric eigenstrains along the nitrided depth according to the volume change accompanying the precipitation of nitrides as well as carbides due to carbon and nitrogen diffusion.
2. Carbon diffusion implies a complex precipitation sequence and thermodynamical evolution which modify the volume change during nitriding.
3. The transformation of initial carbides into nitrides decreases the kinetics of nitriding and is counteracted by the precipitation of cementite. This results in a decrease in volumetric eigenstrains and so residual stresses during nitriding.
4. Owing to carbon diffusion at the diffusion front, the volume fraction of carbides is increased, leading to less volume change when transformed into nitrides and a lower precipitation of semi-coherent nitrides. Consequently,

the maximal residual stresses decreases when time increases.

5. Surface decarburization involves a decrease in the volume fraction of cementite during nitriding leading to an unloading of the surface and thus a decrease in residual stresses.
6. The influence of the developed stress state on the microstructure was observed: the lower the residual stresses in the ferritic matrix, the lower the precipitation of cementite at grain boundaries.
7. Creep, usually used to describe stress relaxation due to coupled diffusion and mechanical loading phenomena, appears to describe the thermo-chemical modifications and so the evolution of the precipitation during nitriding.
8. A volume change calculation is proposed based on the evolution of the volume fraction of precipitates. The calculation is in agreement with a self-consistent scheme for residual stress determination at the microscopic and macroscopic scales.
9. Whereas the strengthening law, linked to the precipitation of fine semi-coherent nitrides, plays a role in the level of residual stresses, volumetric heterogeneities through a nitrided surface and, consequently, the distribution of residual stresses are mainly governed by the thermo-chemical modifications due to nitrogen and carbon diffusion. During nitriding, a surface was subject to mechanical loading–unloading through volume changes.

Acknowledgements

The authors acknowledge Aubert & Duval (Eramet Group) and the Safran Group for their support, as well as CP2M laboratory, Paul Cezanne University, Marseille, for TEM investigations.

References

[1] Jack KH. Heat Treat 1973;4:39.
[2] Totten G, Howes M, Inoue T. Handbook of residual stress and deformation of steel. Materials Park (OH): ASM International; 2002.
[3] Rozendaal HCF, Colijn PF, Mittemeijer EJ. Surf Eng 1985;1:30.
[4] Mittemeijer EJ, Rozendaal HCF, Colijn PF, Van der Schaaf PJ, Furnee RT. In: Proceedings of the conference on heat treatment. Birmingham UK; 1981.
[5] Withers PJ, Bhadeshia HKDH. Mat Sci Tech 2001;17:355.
[6] Barrallier L, Barralis J. In: Proceedings of ICRS4. Baltimore, (MD) USA: Society for Experimental Mechanics Inc.; 1994.
[7] Oettel H, Schreiber G. AWT-Tagunsband "Nitrieren und Nitrocarburieren'. AWT, Wiesbaden, Germany; 1991.
[8] Mittemeijer EJ. In: Proceedings of the symposium sponsored by the heat treatment committee of the metallurgical society of AIME held at the 112th AIME annual meeting. New-York: Metallurgical Society of AIME; 1984.
[9] Vives Diaz NE, Schacherl RE, Zagonel LF, Mittemeijer EJ. Acta Mat 2008;20:228.
[10] Jessner P, Danoix R, Hannoyer B, Danoix F. Ultramicro 2009;109:530.
[11] Barralis J, Castex L, Chaize JC. Mémoires et Etudes Scientifiques Revue de Métallurgie, Décembre 1986. p. 629–642.
[12] Kreft U, Hoffmann F, Hirsch T, Mayr P. Surf Eng 1995;11:61.
[13] Gunther D, Hoffmann F, Hirsch T. HTM 2004;59:18.
[14] Barrallier J, Soto R, Sprauel JM, Charai A. Met Mat Trans A 1997;28:851.
[15] Hirsch TK, Rocha ADS, Ramos FD, Strohaecker TR. Met Mat Trans A 2004;35:3523.
[16] Somers MAJ. J Phys IV France 2004;120:21.
[17] Oettel H, Schreiber G. In: Proceedings of ICRS4. Baltimore, MD USA: Society for Experimental Mechanics Inc.; 1994.
[18] Buchhagen P, Bell T. Comp Mat Sci 1996;7:228.
[19] Daves W, Fischer FD. Mater Sci Forum 1994;163–165:713.
[20] Locquet JN, Barrallier L, Soto R, Charai A. Micro Microanal Microstruct 1997;8:335.
[21] Leroy C, Michel H, Gantois M. J Mat Sci 1986;21:3467.
[22] Leroy C, Michel H, Gantois M. In: Second international conference on heat treatment of material, Associazone Italiana di Metallurgia, Florence, Italy; 1982.
[23] Traskine VY, Bochenkov SE, Skvortsova ZN, Barrallier L. Colloid J 2005;67:106.
[24] Sennour M, Jacq C, Esnouf C. J Mat Sci 2004;39:4533.
[25] Clauss AR, Bischoff E, Hosmani SS, Schacherl RE, Mittemeijer EJ. Met Mat Trans A 2009;40:1923.
[26] Goret V, Phd thesis, Arts & Metiers ParisTech, France; 2006.
[27] Jegou S, Kubler R, Barrallier L, Roch F. In: Proceedings of ICRS8, advances in X-ray analysis, Denver, Colorado USA; 2008 52.
[28] Jegou S, Kubler R, Barrallier L. In: Proceedings of thermech'09, vol. 89–91. Berlin, Germany: Advanced Materials Research; 2010. p. 256.
[29] JCPS-International Center for Diffraction Data, PDF-2; 2002.
[30] Li J, Malis T, Dionne S. Mat Charact 2005.
[31] Goret V, Fabre A, Barrallier L, Vardon P. In: Proceedings of ECRS7, Mat Sci Forum 2006;524–525:285.
[32] Thermo-Calc Software, Stockolm, Sweden.
[33] Ginter C, Torchane L, Dulcy J, Gantois M, Malchere A, Esnouf C, et al. La Metallurgia Italiana 2006;7–8:29.
[34] Mittemeijer EJ, Straver WTM, Colijn PF. Scr Met 1980;14:1189.